

DOI: 10.1002/adfm.200500785

Effect of Hole Mobility Through Emissive Layer on Temporal Stability of Blue Organic Light-Emitting Diodes**

By Sean W. Culligan, Andrew C.-A. Chen, Jason U. Wallace, Kevin P. Klubek, Ching W. Tang,* and Shaw H. Chen*

Light-emitting conjugated oligomers comprising anthracene, naphthalene, and fluorene units have been synthesized to investigate three configurations of blue organic light-emitting diodes (OLEDs) that are designed to identify the origins of device instability. The transient OLED technique is employed to measure hole mobilities, which are found to be 3.1×10^{-4} , 8.9×10^{-5} , and $3.6 \times 10^{-5} \text{ cm}^2 \text{ V}^{-1} \text{ s}^{-1}$ for three different blue-light-emitting model compounds with varying fluorene content. A higher hole mobility through the emissive layer results in a wider recombination zone, which, in turn, is responsible for a longer device lifetime and a lower drive voltage at the expense of luminance yield.

1. Introduction

Since the discovery of efficient organic light-emitting diodes (OLEDs) based on low-molecular-weight compounds^[1] and conjugated polymers,^[2] significant progress in materials and device science has led to the realization of full-color OLEDs with improved efficiencies and lifetimes.^[3] Operational stability, however, is still a major challenge for OLED display technologies.^[4] The stability of green OLEDs containing tris-(8-hy-

droxyquinoline) aluminum (Alq3) has been extensively investigated.^[5] In contrast, the stability of blue OLEDs has remained largely unexplored. While many classes of blue-light emitters have been developed,^[6] the device lifetimes for most of the materials have not been reported to date. Several anthracene derivatives have been demonstrated for use in efficient blue OLEDs with promising stability.^[7] Nevertheless, the reported lifetimes are poor compared to those of state-of-the-art green and red OLEDs. Identification of the key factors influencing device stability is crucial to the realization of superior blue-light-emitting materials and devices.

Fluorene-containing polymers^[8] and oligomers^[9] are an emerging class of blue-light-emitting materials. Efficient UV-to-deep-blue unpolarized and polarized OLEDs have been realized using amorphous and glassy-nematic oligo(fluorene)s,^[10,11] respectively. The OLED lifetimes of blue-light-emitting poly(fluorene)s have been reported without disclosure of the polymer structure.^[12] Oligomers are better suited than polymers to elucidate the effects of chemical structure on OLED lifetime because of their well-defined and uniform molecular structure, as well as superior chemical purity. Additionally, thermal and electrochemical properties of the transport layers,^[13] the location and extent of the recombination zone,^[5c,14] and the presence of charge traps^[15] are all relevant to OLED stability. With the ultimate goal of developing stable blue-light-emitting materials, the present study targets anthracene- and fluorene-containing oligomers to unravel how molecular structure and device architecture affect OLED stability.

2. Results and Discussion

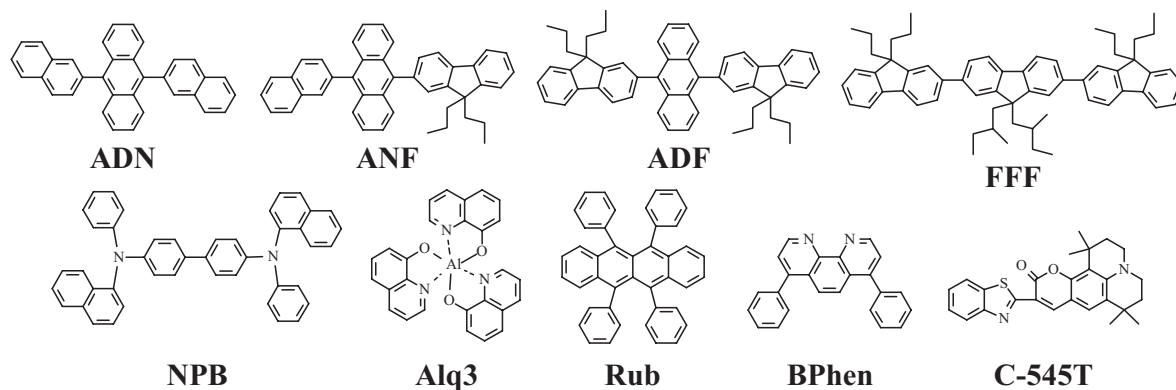
The molecular structures of the model compounds used in this work are shown in Scheme 1. ADN is a known material commonly used as a host in doped blue OLEDs.^[7a] It has two naphthyl moieties substituted in the 9- and 10-positions of the anthracene core. In ANF, one position is substituted with a

[*] Dr. C. W. Tang, Dr. S. H. Chen, S. W. Culligan, A. C.-A. Chen, J. U. Wallace
Department of Chemical Engineering, University of Rochester
240 East River Road, Rochester, NY 14623-1212 (USA)
E-mail: ching.tang@kodak.com; shch@lle.rochester.edu

Dr. C. W. Tang, K. P. Klubek
Display Science and Technology Center, Eastman Kodak Company
1999 Lake Avenue, Rochester, NY 14650-2116 (USA)

Dr. S. H. Chen
Laboratory for Laser Energetics, University of Rochester
240 East River Road, Rochester, NY 14623-1212 (USA)

[**] The authors thank Drs. Ralph Young, Liang-Sheng Liao, and Kathleen Vaeth (Eastman Kodak) and Professor Lewis J. Rothberg of the Department of Chemistry at the University of Rochester for helpful discussions, and Myron Culver and Dustin Comfort (Eastman Kodak) for experimental assistance. Additionally, the contributions of Drs. Andrew Hoteling (MALD/I-TOF-MS) and Craig Swanson (neutron activation analysis), both of Eastman Kodak, are greatly appreciated. The authors are grateful for the financial support provided by the Eastman Kodak Company, the New York State Center for Electronic Imaging Systems, and the National Science Foundation under Grant CTS-0204827 (SHC). Additional funding was provided by the Department of Energy Office of Inertial Confinement Fusion under Cooperative Agreement No. DE-FC03-92SF19460 with the Laboratory for Laser Energetics and the New York State Energy Research and Development Authority (SHC). The support of the DOE does not constitute an endorsement by the DOE of the views expressed in this article. Supporting Information is available online from Wiley InterScience or from the author.



Scheme 1. Molecular structures and symbols of model compounds, transport materials, and dopants.

naphthyl moiety and the other with a fluorene moiety. In ADF, both positions are substituted with fluorene. FFF contains three fluorene moieties without an anthracene core. These model compounds can be considered as a family of compounds with a varying degree of fluorene content, from none in ADN to three fluorene units in FFF. All model compounds were prepared using the Suzuki coupling reaction;^[16] details of the synthesis and assessment of chemical purity are described in the Supporting Information.

The relevant energy levels for these model compounds are listed in Table 1. The half-wave oxidation potentials, $E_{1/2}^{(ox)}$, were measured by cyclic voltammetry and used for the calculation of the highest occupied molecular orbital (HOMO) levels, using a reported linear correlation between the two parameters.^[17] The resultant HOMO levels of ADN, ANF, and ADF are indistinguishable from each other (5.77 ± 0.03 eV), leading to the same hole-injection barrier from NPB to the emissive layers (EMLs) that consist of the three model compounds.

The bandgap energies were estimated from the onset of the absorption spectra in dilute solution (see Supporting Information). The results indicate that ADN, ANF, and ADF have the same bandgap energies (2.97 ± 0.02 eV) within experimental er-

ror. With no anthracene core, FFF shows a higher bandgap energy than ADN, ANF, and ADF. The bandgap energies of the model compounds relative to that of NPB will influence the electroluminescence (EL) spectra if recombination occurs at the interface between the model-compound EMLs and the NPB hole-transporting layer (HTL), as excitons tend to migrate to the lower-energy excited state. Specifically, ADN, ANF, and ADF are expected to be responsible for the emission from OLEDs comprising these model compounds. In contrast, OLEDs consisting of FFF will produce an EL spectrum that originates from NPB.

As shown in Figure 1, evaporated films produced near-UV to blue photoluminescence (PL) upon UV excitation at 360 nm. The film thickness, evaluated using a quartz-crystal microbalance, ranged from 30 to 50 nm. Note that ADN, ANF, and ADF yield identical fluorescence spectra that are attributable to anthracene.^[18] The emission from FFF displays a blue-shift relative to the anthracene compounds and shows vibronic progression similar to other fluorene-containing compounds.^[9b–e,10]

To assess the EL properties of these model compounds, in particular their relative stability in OLED operation, three device structures (I, II, III) were used, as depicted in Figure 2. Device I has a three-layer structure where the model compound forms the EML sandwiched between the NPB HTL and the Alq3 electron-transporting layer (ETL). In Device II, the

Table 1. Half-wave oxidation potentials ($E_{1/2}^{(ox)}$), highest occupied molecular orbital (HOMO) energy levels, and optical bandgaps in dilute solution for the model compounds ADN, ANF, ADF, and FFF, and the hole-transporting material NPB.

Compound	$E_{1/2}^{(ox)}$ [mV] [a]	HOMO [eV] [b]	Bandgap [eV] [c]
NPB	770	5.30	3.10
ADN	1236	5.80	2.99
ANF	1214	5.77	2.98
ADF	1190	5.73	2.96
FFF	1278	5.86	3.20

[a] Relative to Ag/AgCl, determined using 0.5 mM solution in anhydrous CH_2Cl_2 with 0.1 M Et_4NBF_4 as a supporting electrolyte. [b] HOMO levels for ADN and NPB measured by photoemission spectroscopy [7a,17]; HOMO levels of other compounds calculated using a linear correlation with measured $E_{1/2}^{(ox)}$ [17]. The calculated HOMO level for ADN is in agreement with that measured by photoemission spectroscopy. [c] Estimated from the absorption onset of 10^{-5} M solution in UV-grade CH_2Cl_2 .

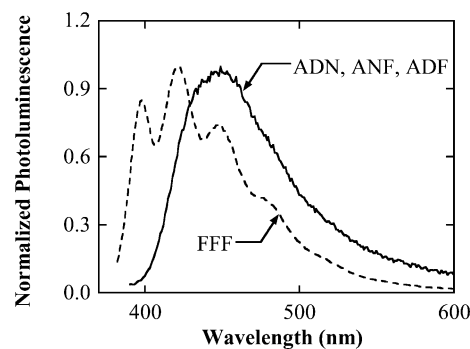


Figure 1. PL spectra of vacuum-evaporated thin films of the model compounds upon UV excitation at 360 nm.

Mg:Ag (2200)	Mg:Ag (2200)	Mg:Ag (2200)
Alq3 (200)	Alq3 (200)	Alq3 (200)
Model (400)	Model (400)	Model (300)
NPB (750)	NPB + Rub (375)	Model + Rub (100)
CF _x (10)	NPB (375)	NPB (750)
ITO	CF _x (10)	CF _x (10)
	ITO	ITO
I	II	III

Figure 2. OLED device structures employed to study EL performance and device lifetime, with layer thicknesses specified in angstroms. ITO: indium tin oxide.

NPB HTL is doped with rubrene (Rub in Scheme 1) at a concentration of 10%. This device structure is used to probe the location of the carrier-recombination zone and the range of electron and/or hole transport in the model compound. In Device III, a portion of the EML adjacent to the NPB HTL is doped with 5% rubrene. This device structure with a partially doped EML has been commonly used to improve the efficiency and stability of OLED devices and is used here to assess structure–property relationships for the model compounds as host materials. For all the devices used in this study, ITO modified with CF_x^[19] has been used as the anode, while the cathode was Mg:Ag.

Table 2 summarizes the EL characteristics and Figure 3 shows the corresponding EL spectra for Devices I–III. Several trends correlating with the molecular structure of the model compounds are noted: 1) the drive voltage increases in the order ADN < ANF < ADF; 2) the current efficiency increases in the same order; and 3) the half-life, in contrast, decreases in the order ADN > ANF > ADF. In addition, distinct features are also noted in the EL spectra that can be correlated with the

Table 2. Summary of OLED performance for Devices I–III at current density, $j = 20 \text{ mA cm}^{-2}$; half-life measured at $j = 40 \text{ mA cm}^{-2}$. CIE: Commission Internationale de l’Eclairage.

	Drive voltage	Efficiency	CIE coordinates	Device half-life
	[V]	[cd A^{-1}]	(x, y)	[h]
Device I				
ADN	8.8	0.69	(0.163, 0.137)	303.1
ANF	9.2	0.70	(0.151, 0.098)	136.7
ADF	9.5	0.85	(0.149, 0.084)	100.4
FFF [a]	13.4	0.37	(0.161, 0.126)	10.9
Device II				
ADN	8.2	2.98	(0.470, 0.474)	1011.1
ANF	8.6	3.16	(0.469, 0.461)	746.4
ADF	9.5	3.42	(0.473, 0.453)	279.5
Device III				
ADN	7.1	2.24	(0.437, 0.487)	1012.4
ANF	7.8	3.14	(0.468, 0.502)	476.0
ADF	9.1	3.24	(0.455, 0.494)	225.5

[a] NPB emitter instead of FFF emitter.

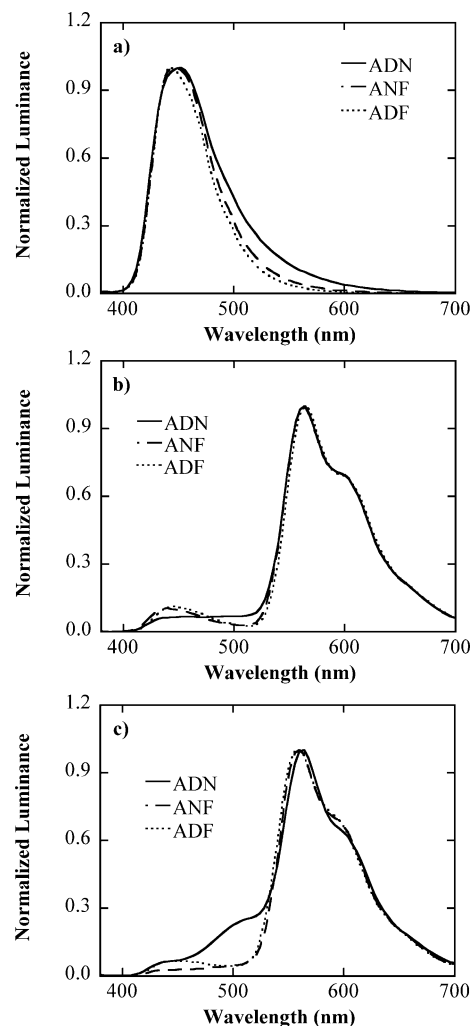


Figure 3. Normalized EL spectra at $j = 20 \text{ mA cm}^{-2}$ for a) Device I devices; b) Device II devices; c) Device III devices comprising ADN, ANF, and ADF, all providing evidence in support of a varying recombination zone width.

molecular structures of the model compounds. For Device I, the EL emission spectra are broad and peak around 460 nm, indicating that they are largely due to emission from the model compounds. However, the spectrum of the ADN device is somewhat broader than those of the ANF and ADF devices at long wavelengths ($\sim 550 \text{ nm}$), suggesting that there is an additional contribution to the EL emission from the green-light-emitting Alq3 ETL. Device I containing FFF displays featureless blue EL, in contrast to the structured PL shown in Figure 1. This emission was found to arise from NPB, suggesting severe hole accumulation at the NPB/FFF interface resulting in NPB EL because of its smaller bandgap compared to FFF, as elucidated from the bandgap energies presented in Table 1.

For Devices II and III, the EL spectra are dominated by the orange emission ($> 550 \text{ nm}$) from rubrene while blue emission attributable to the model compounds is present at a much lower intensity. The ADN devices appear to be different in that the relative EL emission is higher in the green spectral region ($\sim 500 \text{ nm}$) compared to the ANF and ADF devices, consistent

with Device I. These observations can be understood by assuming that the extent of the recombination zone is reduced by the decreasing hole mobility as naphthalene is replaced by fluorene in the model compounds. This assumption will be validated by the hole-mobility values obtained from transient EL measurements described in what follows.

Transient OLEDs were fabricated to measure the hole mobility. Semitransparent platinum anodes were sputter-coated and treated with CF_x to reduce the device resistance and improve hole injection.^[19] A high-electron-mobility Li-doped ETL^[20] was used to ensure that the transient response was determined by hole transport in the model compound. Figure 4a shows the steady-state EL spectrum, with the device structure shown in the inset.

Contrary to typical transient OLEDs,^[21] the frequency-domain response was used to measure the hole mobility.^[22] The decrease in EL intensity at high frequencies of the DC voltage pulses was apparently the result of fewer holes reaching the Alq3 + C-545T layer. The hole-transit time was estimated from the intercept of the tangents of the light-output versus frequency curves (see Experimental section). The mobility was then calculated based on the film thickness and the applied field. To validate this approach, a 3500 Å film of NPB was used as the model layer in a transient OLED. Based on the frequency-dependent EL quenching (see Supporting Information), the mobility was $9.6 \times 10^{-4} \text{ cm}^2 \text{ V}^{-1} \text{ s}^{-1}$ at an applied field of $2.3 \times 10^5 \text{ V cm}^{-1}$, a value that agrees with the time-of-flight transient photocurrent measurement, $(8.8 \pm 2.0) \times 10^{-4} \text{ cm}^2 \text{ V}^{-1} \text{ s}^{-1}$.^[23] With confidence based on the results obtained for NPB, 3000 Å films of the model compounds were tested in transient OLEDs. The frequency-dependent EL quenching observed for these devices is shown in Figure 4b.

On the basis of Figure 4b, the hole mobilities are evaluated to be 3.1×10^{-4} , 8.9×10^{-5} , and $3.6 \times 10^{-5} \text{ cm}^2 \text{ V}^{-1} \text{ s}^{-1}$ for ADN, ANF, and ADF, respectively. Repeated experiments with ADN yielded an experimental uncertainty of $\pm 7\%$ in the mean. It is evident that the mobility decreases incrementally with each substitution of naphthalene by fluorene, thereby narrowing the recombination zone. The observed effect of the fluorene content in the model compounds on hole mobility is

limited to the three model compounds in amorphous films, as hole mobility is known to depend on film morphology and molecular orientation. A case in point is the reported hole mobilities on the order of $10^{-2} \text{ cm}^2 \text{ V}^{-1} \text{ s}^{-1}$ measured by the time-of-flight technique for glassy-nematic oligofluorene films.^[24] Additional evidence in support of the hole-transport limitation is provided in Figure 5, in which the current-density dependence of Device III containing ADN is presented. At the lowest current density (j) of 0.5 mA cm^{-2} the spectrum is dominated by Alq3 emission, suggesting that hole transport across the ADN layer is facile even at low voltages. As the current density increases, the primary emission originates from rubrene with an increasing contribution from ADN emission at 448 nm. In contrast, the EL spectra for Device III containing ANF and ADF, which are shown in the Supporting Information, are essentially independent of current density from 0.5 to 100 mA cm^{-2} .

The increase in the drive voltage from ADN to FFF devices can be attributed to the hole-transport limitation in the model compound with increasing fluorene content. The fact that the same trend is observed for the three types of devices indicates that the voltage across the model-compound layer is significant and the effect of the molecular structure on the electrical impedance of this layer is reflected in the overall drive voltage on the OLED device. Based solely on the drive voltages, it is not possible to determine if different electron mobilities affect the

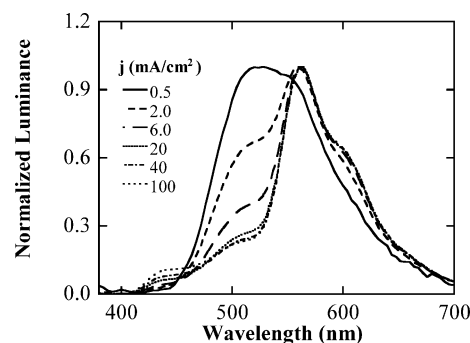


Figure 5. Current-density (j) dependence of the EL spectrum of Device III with ADN, showing favorable hole transport at low current densities.

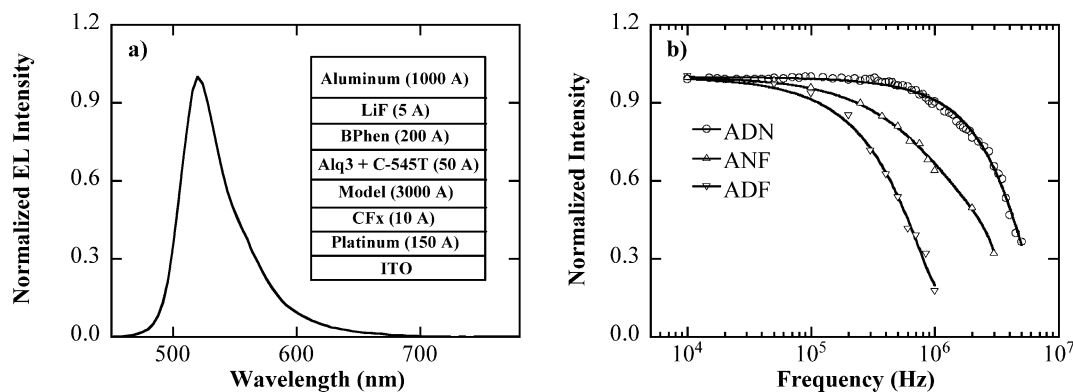


Figure 4. a) Steady-state EL spectrum of a typical transient OLED. Inset: transient OLED device structure. b) Frequency-dependent EL quenching upon application of 8 V square-wave DC voltage pulses of increasing frequency, 50% duty cycle; solid curves represent the best fits to polynomials.

device performance. However, if the difference in electron mobility is a contributing factor, ADF should be a better electron-transporting medium than ADN and ANF based on the recombination-zone width, which is inconsistent with the higher drive voltages for Devices I–III containing ADF.

The increase in efficiency from ADN to ADF devices can also be understood in light of the transport limitation. The EL spectra imply that recombination occurs primarily at the hole HTL/EML interface, where it is expected to contribute more efficiently to EL emission than that at the EML/ETL interface. A reduced hole mobility would therefore result in a higher EL efficiency because of a greater extent of recombination at the HTL/EML interface. Conversely, an electron-transporting limitation would result in a lower EL efficiency. Thus, the observed efficiency trend is consistent with ADN supporting hole transport better than ANF and ADF.

The EL spectra shown in Figure 3 are also consistent with hole mobility descending in the order $\text{ADN} > \text{ANF} > \text{ADF}$. These spectra show different degrees of contribution to the overall EL emission from the Alq3 electron-transporting layer, which can be correlated with the structure of the model compound. For Device I comprising undoped model compounds, the EL spectrum for ADN is distinctly broader than that of ANF and ADF despite the identical PL spectra. This broadening in the long-wavelength region can be attributed to higher emission intensity from the Alq3 layer in the ADN device than in the ANF and ADF devices. It shows that ADN is a better hole-transporting medium than ANF and ADF, resulting in more holes reaching the Alq3 interface in the OLED device. For Devices II and III, the EL spectra are dominated by orange emission from rubrene with a much smaller amount of blue emission from the model compounds. As in Device I, emission from the Alq3 ETL is appreciable in the devices with ADN as a result of the higher hole mobility in ADN than in ANF or ADF.

The differences in hole mobility can also explain the relative stability of the devices. The Alq3 emission described above provides evidence that the width of the recombination zone increases with hole mobility, thereby allowing more ADN than ANF and ADF molecules to participate in the recombination process. Therefore, even if the degradation rate per molecule were the same regardless of the molecular structure, the operational lifetime of the ADN device would be longer compared to the ANF and ADF devices, in which the recombination zone is more confined towards the NPB HTL because of reduced hole mobility in ANF and ADF compared to ADN.

Devices II and III were designed to study the dependence of the EL characteristics on the charge transport and recombination in the model compounds using a doped device structure. Rubrene was chosen as the dopant because its orange emission is easily differentiated from the blue emission of the model compounds, and, thus, can be used to locate the recombination zone. In Device II rubrene was doped into the NPB HTL, whereas in Device III it was doped into the model-compound EML. For Device II, rubrene is not expected to significantly affect the transport of holes in NPB because the HOMO level of rubrene at 5.36 eV^[25] is almost isoenergetic with that of

NPB, which would make it ineffective as a hole trap. This, in fact, is the case, as inferred from the similar drive-voltage trend and magnitudes for Devices I and II, as shown in Table 2. Doping the model compound with rubrene in Device III reduces the operating voltage compared to Device I by providing an energetically favorable site for holes on the EML side, as the HOMO of rubrene is substantially lower than those of the model compounds (Table 1).

Table 2 shows consistent trends in drive voltage, efficiency, and lifetime across the three OLED configurations, which provides strong evidence that the results are not related to device structure. The contribution of the green emission from Alq3 to the EL spectra shown in Figure 3 can be used as a measure of the width of the recombination zone, which decreases in the order $\text{ADN} > \text{ANF} > \text{ADF}$ in all three device configurations. Carrier accumulation at the HTL/EML interface because of large energy barriers or drastic changes in mobility would be expected to confine recombination close to this interface. The HOMO levels of the model compounds, however, suggest that the energy barriers for hole injection are nearly identical, further reinforcing the notion that the hole mobilities of the model compounds have the most substantial impact on the recombination-zone width and, hence, the device efficiency and lifetime. The effects of chemical structure on transport properties and OLED efficiency have been demonstrated previously without disclosing stability.^[26] However, to the best of our knowledge, this is the first report directly correlating molecular structure, carrier-transport properties, and OLED lifetime.

3. Conclusions

In summary, blue-light-emitting model compounds ADN, ANF, and ADF with varying fluorene content were synthesized for integration in three OLED device configurations to furnish new insight into the factors affecting device efficiency and lifetime. Key findings are recapitulated as follows:

- 1) The three model compounds have the same HOMO energy level within experimental error and, hence, there is no variation in the hole-injection barrier from NPB to the emissive layer comprising the model compounds. Furthermore, all three model compounds show the same PL spectra characteristic of the anthracene central unit.

- 2) The varying contribution of green emission from Alq3 as the electron-transporting layer to the EL spectra is attributable to the difference in hole mobility through the emissive layer, which could affect the width of the recombination zone. The hole mobilities were measured using the transient OLED technique to be 3.1×10^{-4} , 8.9×10^{-5} , and $3.6 \times 10^{-5} \text{ cm}^2 \text{ V}^{-1} \text{ s}^{-1}$ for ADN, ANF, and ADF, respectively.

- 3) The higher the hole mobility through the emissive layer, the wider the recombination zone. A wider recombination zone is found to be responsible for a longer device lifetime and a lower drive voltage at the expense of luminance yield. To the best of our knowledge, this is the first demonstration of the effect of hole mobility through the emissive layer on OLED device lifetime.

4. Experimental

4.1. Materials Synthesis

All solvents, chemicals, and reagents for synthesis of the model compounds were used as received from commercial sources with the exception of tetrahydrofuran and 9-bromoanthracene, which had been distilled over sodium/benzophenone and recrystallized from ethanol, respectively. 9,9-bis(*n*-propyl)-fluoren-2-yl-boronic acid and 2,7-dibromo-9,9-bis(2-methylbutyl)fluorene were prepared following previously reported procedures [9c]. The model compounds were prepared using the Suzuki coupling reaction [16]. See the Supporting Information for details of synthesis, purification, and structure identification.

4.2. Solution Electrochemistry and UV-vis Spectroscopy

Cyclic voltammetry was performed in 0.5 mM solutions of the substrates with a cell potentiostat (Bioanalytical Systems Epsilon). All oxidation measurements were carried out in argon-purged anhydrous CH₂Cl₂ containing 0.1 M tetraethyl ammonium tetrafluoroborate (Et₄NBF₄) as a supporting electrolyte. Platinum disk, platinum wire, and Ag/AgCl (saturated) were used as the working, counter, and reference electrodes, respectively. Absorption spectra of dilute solutions were collected using a diode-array spectrophotometer (HP 8453E). The optical bandgaps were determined from the absorption onset of 0.01 mM solutions in UV-grade CH₂Cl₂.

4.3. Thin-Film Preparation and PL Spectroscopy

Thin films were prepared by vacuum evaporation at a base pressure of 5×10^{-6} Torr (1 Torr \approx 133 Pa) or lower. The film thickness was measured with a calibrated quartz-crystal microbalance during deposition. Fluorescence spectra were collected with a spectrofluorimeter (Quanta Master C60SE, Photon Technology International) with 360 nm excitation and detection in a straight-through geometry.

4.4. OLED Fabrication and Characterization

Patterned indium tin oxide (ITO)-coated glass substrates (Polytronix) were thoroughly cleaned, treated with oxygen plasma, and coated with a thin layer of CF_x [19] prior to use. Organic materials were sublimed prior to device experiments. OLEDs were prepared in a multiple-source thermal evaporation system at a base pressure of 5×10^{-6} Torr or lower. The deposition rate, controlled using a deposition controller (Infineon IC/5), was 4 \AA s^{-1} for all organic materials except dopants, which were coevaporated at an appropriate rate to obtain the desired doping level. The rubrene doping level was 10 and 5 % in Devices II and III, respectively. The Mg:Ag cathode was coevaporated at rates of 10 and 1 \AA s^{-1} , respectively. All OLEDs were encapsulated prior to characterization using a source-measure unit (Keithley 2400) and a spectroradiometer (PhotoResearch PR650). To determine the OLED lifetimes, the devices were driven at a constant DC current density of 40 mA cm^{-2} while the emission intensity was monitored using a silicon photodiode.

4.5. Transient-OLED Fabrication and Characterization

ITO-coated glass substrates were sputter-coated with 1000 Å of chromium to lower the resistivity. Semitransparent platinum (150 Å) was sputter-coated in the anode region before the metallized substrate was treated with CF_x. Organic layers were deposited as described

above. The C-545T doping level in the thin Alq₃ layer was 2.5 %. A thin LiF layer was deposited at a rate of 0.1 \AA s^{-1} to improve electron injection [22a]. The aluminum cathode was deposited at a rate of 15 \AA s^{-1} through a shadow mask, resulting in a device area of $\sim 0.005 \text{ cm}^2$ to improve the resistance-capacitance (RC) response. A function generator (HP 8116 A) was used to apply 8.0 V DC square wave voltage pulses. Emitted light was collected by a silicon photodiode (UDT). Voltage pulses and light output were recorded by a digitizing oscilloscope (Tektronix TDS 460A). The normalized light intensity versus frequency curve was used to determine the transit time τ_{tr} . The intercept of the tangent to this curve at a normalized light intensity of 0.5 with the horizontal axis at the normalized intensity of 1.0 defined the frequency f for the calculation of τ_{tr} ($= 1/(2f)$), in which the factor two accounts for the 50 % duty cycle. The mobility was then calculated using $\mu = d/(\tau_{tr}E)$, with d denoting the film thickness and E the applied field, assuming the field drops across the model compound and neglecting the built-in potential.

Received: November 9, 2005

Final version: December 17, 2005

Published online: June 14, 2006

- [1] C. W. Tang, S. A. VanSlyke, *Appl. Phys. Lett.* **1987**, *51*, 913.
- [2] J. H. Burroughes, D. D. C. Bradley, A. R. Brown, R. N. Marks, K. Mackay, R. H. Friend, P. L. Burn, A. B. Holmes, *Nature* **1990**, *347*, 539.
- [3] Recent reviews: a) Y. Shirota, *J. Mater. Chem.* **2005**, *15*, 75. b) B. W. D'Andrade, S. R. Forrest, *Adv. Mater.* **2004**, *16*, 1585. c) C.-T. Chen, *Chem. Mater.* **2004**, *16*, 4389.
- [4] H. Aziz, Z. D. Popovic, *Chem. Mater.* **2004**, *16*, 4522.
- [5] a) H. Aziz, Z. D. Popovic, N.-X. Hu, A.-M. Hor, G. Xu, *Science* **1999**, *283*, 1900. b) H. Aziz, Z. D. Popovic, *Appl. Phys. Lett.* **2002**, *80*, 2180. c) A. B. Chwang, R. C. Kwong, J. J. Brown, *Appl. Phys. Lett.* **2002**, *80*, 725. d) Z. D. Popovic, H. Aziz, N.-X. Hu, A. Ioannidis, P. N. M. dos Anjos, *J. Appl. Phys.* **2001**, *89*, 4673.
- [6] a) C. Adachi, T. Tsutsui, S. Saito, *Appl. Phys. Lett.* **1990**, *56*, 799. b) C. Hosokawa, H. Higashi, H. Nakamura, T. Kusumoto, *Appl. Phys. Lett.* **1995**, *67*, 3853. c) C. C. Wu, Y. T. Lin, H. H. Chiang, T. Y. Cho, C. W. Chen, K. T. Wong, Y. L. Liao, G. H. Lee, S. M. Peng, *Appl. Phys. Lett.* **2002**, *81*, 577. d) L.-H. Chan, R.-H. Lee, C.-F. Hsieh, H.-C. Yeh, C.-T. Chen, *J. Am. Chem. Soc.* **2002**, *124*, 6469. e) Y. Z. Wu, X. Y. Zheng, W. Q. Zhu, R. G. Sun, X. Y. Jiang, Z. L. Zhang, S. H. Xu, *Appl. Phys. Lett.* **2003**, *83*, 5077. f) A. P. Kulkarni, A. P. Gifford, C. J. Tonzola, S. A. Jenekhe, *Appl. Phys. Lett.* **2005**, *86*, 061 106. g) S.-J. Yeh, M.-F. Wu, C.-T. Chen, Y.-H. Song, Y. Chi, M.-H. Ho, S.-F. Hsu, C. H. Chen, *Adv. Mater.* **2005**, *17*, 285.
- [7] a) J. Shi, C. W. Tang, *Appl. Phys. Lett.* **2002**, *80*, 3201. b) M.-T. Lee, H.-H. Chen, C.-H. Liao, C.-H. Tsai, C. H. Chen, *Appl. Phys. Lett.* **2004**, *85*, 3301. c) S.-Y. Ni, X. R. Wang, Y. Z. Wu, H. Y. Chen, W. Q. Zhu, X. Y. Jiang, Z. L. Zhang, R. G. Sun, *Appl. Phys. Lett.* **2004**, *85*, 878. d) M.-T. Lee, C.-H. Liao, C.-H. Tsai, C. H. Chen, *Adv. Mater.* **2005**, *17*, 2493.
- [8] a) D. Neher, *Macromol. Rapid Commun.* **2001**, *22*, 1365. b) U. Scherf, E. J. W. List, *Adv. Mater.* **2002**, *14*, 477.
- [9] a) G. Klärner, R. D. Miller, *Macromolecules* **1998**, *31*, 2007. b) Y. Geng, D. Katsis, S. W. Culligan, J. J. Ou, S. H. Chen, L. J. Rothberg, *Chem. Mater.* **2002**, *14*, 463. c) Y. Geng, S. W. Culligan, A. Trajkovska, J. U. Wallace, S. H. Chen, *Chem. Mater.* **2003**, *15*, 542. d) Y. H. Geng, A. Trajkovska, D. Katsis, J. J. Ou, S. W. Culligan, S. H. Chen, *J. Am. Chem. Soc.* **2002**, *124*, 8337.
- [10] a) K. T. Wong, Y.-Y. Chien, R.-T. Chen, C.-F. Wang, Y.-T. Lin, H.-H. Chiang, P.-Y. Hsieh, C.-C. Wu, C. H. Chou, Y. O. Su, G.-H. Lee, S.-M. Peng, *J. Am. Chem. Soc.* **2002**, *124*, 11 576. b) C.-C. Wu, Y.-T. Lin, K.-T. Wong, R.-T. Chen, Y.-Y. Chien, *Adv. Mater.* **2004**, *16*, 61. c) T.-C. Chao, Y.-T. Lin, C.-Y. Yang, T. S. Hung, H.-C. Chou, C.-C. Wu, K.-T. Wong, *Adv. Mater.* **2005**, *17*, 992.

- [11] S. W. Culligan, Y. Geng, S. H. Chen, K. P. Klubek, K. M. Vaeth, C. W. Tang, *Adv. Mater.* **2003**, *15*, 1176.
- [12] a) S. I. E. Vulto, M. Büchel, P. C. Duineveld, F. Dijkman, M. Hack, M. Kilitziraki, M. M. de Kok, E. A. Muelenkamp, J.-E. J. M. Rubingh, P. van de Weijer, S. H. P. M. de Winter, *Proc. SPIE-Int. Soc. Opt. Eng.* **2004**, *5214*, 40. b) M. Leadbeater, N. Patel, B. Tierney, S. O'Connor, I. Grizzi, C. Towns, *Soc. Inf. Displ. Int. Symp.* **2004**, *35*, 162.
- [13] a) Y. Shirota, K. Okumoto, H. Inada, *Synth. Met.* **2000**, *111–112*, 387. b) J.-R. Gong, L.-J. Wan, S.-B. Lei, C.-L. Bai, X.-H. Zhang, S.-T. Lee, *J. Phys. Chem. B* **2005**, *109*, 1675. c) C. Adachi, K. Nagai, N. Tamoto, *Appl. Phys. Lett.* **1995**, *66*, 2679. d) G. Vamvounis, H. Aziz, N.-X. Hu, Z.-D. Popovic, *Synth. Met.* **2004**, *143*, 69.
- [14] a) V.-E. Choong, S. Shi, J. Curless, C.-L. Shieh, H. C. Lee, F. So, J. Shen, J. Yang, *Appl. Phys. Lett.* **1999**, *75*, 172. b) J.-H. Lee, C.-I. Wu, S.-W. Liu, C.-A. Huang, Y. Chang, *Appl. Phys. Lett.* **2005**, *86*, 103 506.
- [15] a) W. Riess, H. Riel, T. Beierlein, W. Brütting, P. Müller, P. F. Seidler, *IBM J. Res. Dev.* **2001**, *45*, 77. b) D. Y. Kondakov, J. R. Sandifer, C. W. Tang, R. H. Young, *J. Appl. Phys.* **2003**, *93*, 1108. c) D. Y. Kondakov, *J. Appl. Phys.* **2005**, *97*, 024503.
- [16] N. Miyaura, A. Suzuki, *Chem. Rev.* **1995**, *95*, 2547.
- [17] B. W. D'Andrade, S. Datta, S. R. Forrest, P. Djurovich, E. Polikarpov, M. E. Thompson, *Org. Electron.* **2005**, *6*, 11.
- [18] G. Klärner, M. H. Davey, W.-D. Chen, J. C. Scott, R. D. Miller, *Adv. Mater.* **1998**, *10*, 993.
- [19] S. W. Tong, C. S. Lee, Y. Lifshitz, D. Q. Gao, S. T. Lee, *Appl. Phys. Lett.* **2004**, *84*, 4032.
- [20] a) J. Kido, T. Matsumoto, *Appl. Phys. Lett.* **1998**, *73*, 2866. b) D. Grozea, A. Turak, X. D. Feng, Z. H. Lu, D. Johnson, R. Wood, *Appl. Phys. Lett.* **2002**, *81*, 3173.
- [21] a) C. Hosokawa, H. Tokailin, H. Higashi, T. Kusumoto, *Appl. Phys. Lett.* **1992**, *60*, 1220. b) C. Hosokawa, H. Tokailin, H. Higashi, T. Kusumoto, *Appl. Phys. Lett.* **1993**, *63*, 1322. c) S. Barth, P. Muller, H. Riel, P. F. Seidler, W. Riess, H. Vestweber, H. Bassler, *J. Appl. Phys.* **2001**, *89*, 3711. d) A. G. Mückl, S. Berleb, W. Brütting, M. Schwoerer, *Synth. Met.* **2000**, *111–112*, 91. e) S. C. Tse, H. H. Fong, S. K. So, *J. Appl. Phys.* **2003**, *94*, 2033.
- [22] A. J. Pal, R. Österbacke, K.-M. Källman, H. Stubb, *Appl. Phys. Lett.* **1997**, *70*, 2022.
- [23] Z. Deng, S. T. Lee, D. P. Webb, Y. C. Chan, W. A. Gambling, *Synth. Met.* **1999**, *107*, 107.
- [24] L.-Y. Chen, W.-Y. Hung, Y.-T. Lin, C.-C. Wu, T.-C. Chao, T.-H. Hung, K.-T. Wong, *Appl. Phys. Lett.* **2005**, *87*, 112 103.
- [25] S. B. Lee, T. Yasuda, M.-J. Yang, K. Fujita, T. Tsutsui, *Mol. Cryst. Liq. Cryst.* **2003**, *405*, 67.
- [26] a) G. Yu, S. Yin, Y. Liu, J. Chen, X. Xu, X. Sun, D. Ma, X. Zhan, Q. Peng, Z. Shuai, B. Tang, D. Zhu, W. Fang, Y. Luo, *J. Am. Chem. Soc.* **2005**, *127*, 6335. b) L.-S. Yu, S.-A. Chen, *Adv. Mater.* **2004**, *16*, 744.